International Journal of Chemical and Biochemical Sciences
(ISSN 2226-9614)

Journal Home page: www.iscientific.org/Journal.html

Radio graphical and Histological Assessment of Nano-aragonite When Used as a Bone Graft Substitute in Rabbits (In Vivo Animal Study)

Mai Hamdy [1], Huda Elgendi [2], Fatma Adel Saad [3], Nelly mohamed abdelsalam[4], Asmaa Yousry Abdalla [5]

[1]*Associate professor of Endodontics, Faculty of Dentistry, Suez Canal University, Ismailia city, Egypt*

[2]*Assistant professor of dental biomaterials, Faculty of Dentistry, Deraya University, Minia, Egypt*

[3]*Associate professor of oral biology, Faculty of Dental Medicine, King Salman International University-Egypt*

[4] *Associate professor of endodontics, Faculty of Dentistry, Suez Canal University, Ismailia city, Egypt*

[5] *Associate professor of Oral Radiology, College of Dentistry, Suez Canal University, Ismailia, Egypt*

Abstract

To evaluate histologically and radio graphically the osseous regeneration of intrabony defect in rabbits treated with mineral trioxide aggregate (MTA) and nano-aragonite (NPCC). 10 males New Zeland rabbits were generally anesthetized and two non-critical size bone defects [5 mm diameter] were crafted bilaterally inside the femur bone. Animals were divided into groups I &II sacrificed after 14 & 28 days respectively. Each group divided into subgroup (a) received MTA treatment for left femur defect, and subgroup (b) received NPCC treatment for right femur defect. MTA & NPCC treated defects were histologically and radio graphically examined. Both NPCC and MTA treated femur defects showed a significant increase (P value <0.001) in the bone density after 28 days when compared to the treated bone defects after 14 days of treatment respectively. Moreover, The NPCC treated defects revealed a high significant increase (P value <0.001) in bone density when compared to MTA treated defects in all periods. Nanoaragonite possesses a higher osteogenic and mineralization potential than MTA in non-critical sized defects. Nano aragonite has a promising effect when used as natural bone substitute.

Keywords: Nanoaragonite, MTA, Bone graft, Intrabony defect, Rabbit.

Full length article **Corresponding Author*, e-mail: *mai_hamdy@dent.suez.edu.eg*

1. Introduction

Several surgical methods employing biological or synthetic bone replacements have been developed to promote the healing of bone defects with new tissue that closely resembles the original tissue in both structure and function [1-2]. The ideal graft material should gradually replace bone tissue and possess osteoinductive, osteoconductive, non-antigenic, non-carcinogenic, and biocompatible properties [3]. In previous studies [4], the use of homografts and xenografts showed several limitations, including restricted bioavailability, rejection of tissue, possible contamination by prion or virus, and the need for immunosuppressive medications [5]. However, because of their high levels of histocompatibility and the presence of a three-dimensional porous matrix that contains vital osteoconductive elements like growth factors, osteoprogenitor cells, and bone morphogenic proteins, auto grafts are frequently regarded as the best option for bone repair [6]. However, these grafts have been associated with surgical complications in the past, such as donor site morbidity, scarring, bleeding, irritation, bacterial contamination, and chronic pain [7-8].

They also include removing bone from areas such as the iliac, mandibular ramus, or chin during surgical procedures. Synthetic bone substitutes, also known as alloplastic bone repairs, are frequently utilized as substitutes for auto grafts since they are easily accessible and do not require a donor location [9]. Despite these positive characteristics, prior researches have shown that alloplastic materials—such as synthetic hydroxyapatites and bioceramics cannot effectively heal critical-sized calvarial injuries in rats and rabbits, among other animal models [10]. To get around these restrictions, a lot of researches have gone

into creating new biocompatible organo-biomaterials, like low-temperature hydroxyapatite, tricalcium phosphate (TCP), and natural hydroxyapatite (HA) [11-12]. Despite the high biocompatibility and osteoconductivity of synthetic hydroxyapatite (HAp) bioceramic, there is a growing focus on carbonated HAp derived from natural sources such as seashells, nacre, and cuttlefish. These natural sources are more akin to the chemical composition of natural bone due to their lack of stoichiometry and the presence of various ion traces including $CO3^{2-}$, Na, Mg, Fe, F, and Cl. Cuttlefish bone, in particular, has garnered attention as an affordable natural source of HAp with high porosity (90%), suitable pore size (200-600µm), and interconnectivity. However, it exhibits poor mechanical properties, a common trait among various forms of HAp. Previous efforts have involved transforming cuttlefish's aragonite into HAp and then coating it with a biocompatible polymer such as polycaprolactone (PCL) [13-14]. Mineral Trioxide Aggregate (MTA) stands out as a promising option for bone-regenerating biomolecules. This biocompatible substance has a wide range of applications, including direct pulp capping of teeth with asymptomatic carious and non-carious pulp exposures. MTA is beneficial for bone healing due to its structure, which promotes rapid cell proliferation and adherence [11].

The drawbacks of MTA involve challenges with inserting it into root-end cavities and the potential for perforations due to its sandy texture and extended setting time. These factors may lead to solubility, disintegration, or displacement from the root-end cavity, prompting researchers to explore the effects of incorporating other compounds into MTA to address these issues [15]. Recent research have demonstrated the advantages of adding nano-particulate calcium carbonate (NPCC or Nano-aragonite), which is categorized as a setting accelerator nanoadditive, to MTA. According to some researchers, nanoparticles (NPs) alter the hydration process, increase fluidity and workability, and fill voids; nanofiller effect) [16]. Hence, we hypothesized that nano-aragonite might make strides in bone recuperating, which in turn may promote the recovery of bone tissue. Consequently, the objective of this study was to assess the bony repair of intraosseous defect in rabbits treated with aragonite nano-particles compared with MTA at both histological and radiographic levels.

2. Materials and Methods

2.1. Ethical statement

This in-vivo study was conducted after the approval of the ethical committee (Approval number: 537/2022), Faculty of Dentistry, Suez Canal University. The Institutional Animal Care approved all animal experiments. All methods were accomplished in strict accordance with the relevant (ARRIVE) guidelines and regulations of Helsinki Declaration for Animal Use.

2.2. Materials

A- Preparation and characterization of nano-aragonite powder (NPCC)

Cuttle fish bones were purchased from local sea food supplier (Nano-Gate - Nasr City - 25 Ibrahium Abou El Naga St. – Cairo – Egypt). The lamellae portion of the cuttlefish bone was ground into a powder using a mortar to produce the $CaCO_3$. After that, the dry powder was processed to extract the $CaCO_3$ using a ball mill (Planetary-ball-mill-pm-400) set for 8 hours at 350 rpm and intervals of 3 minutes [17]. The TEM micrographs of NPCC (Figs. 1A, 1B, 1C& 1D) revealed relatively regular spherical particles with fairly uniform sizes with average particle size 25±5nm. Some are scattered and others are clustered together as seen in (Fig. 1C). SEM micrograph (Figs. 1E & 1F) presented variable surface morphologies where they exhibited diverse forms of "rod shaped" and "spherical" patterns. Most of the crystals were agglomerated and clumped together. EDX analysis was performed to determine the elemental composition of NPCC. Briefly, essential elements (Ca, O2 and C) were observed as shown in (Fig. 1G) by weight percentage: oxygen, calcium, carbon (58.26, 21.93 and 16.21 respectively), besides, some trace percentages of chloride and sodium.

B- Preparation of Mineral Trioxide Aggregate (MTA)

White MTA was mixed according to manufacturer's instructions at a powder-to-liquid ratio of 3:1[18] [Angelus Soluçõe Odontológicas, Londrina, and Paraná, Brazil].

2.3. Methods

2.3.1. Animals

Ten male white New Zealand rabbits (weighed 3.5–4 kg) were utilized, housed in the animal house - Faculty of dentistry - Suez Canal University, and given a week to acclimate to the experiment. Animals had unlimited access to water and standard rodent diet under a 12-hour light/dark cycle at a room temperature of 18–22°C and a relative humidity of 55–65%. The rabbits were placed individually in stainless steel cages 30 x 36 square inches to ensure proper healing and prevent wound infection. Animals were kept under the supervision of the attending veterinarian [19].

2.3.2. Sample size calculation

Sample size calculation was performed using G*Power version 3.1.9.2, Faul *et al,* [20] University Kiel, Germany. Copyright (c) 1992-2014. The effect size *d* was **1**.6 (large) according to the previous studies with alpha (α) level of 0.05 and Beta (β) level of 0.05, i.e., power = 95%; the estimated sample size (n) should be 20 samples and will be divided equally into two main groups (10 samples/group).

2.3.3. Anesthesia and Surgery

All animals were received general anesthesia by intramuscular injections of 0.35 ml/kg of ketamine hydrochloride and 0.15 ml/kg of xylazine hydrochloride. On the first day of the experiment, the surgical field was carefully cleaned and disinfected usingz 10% Povidone Iodine solution [Betadine, Purdue Pharma, and Norwalk, CT]. A 0.9 ml local anesthetic injection (lidocaine 2%, Parhawk Laboratories, USA) was directed to the surgical site before a 1.5 cm length incision was made with a number 15 blade. Following a severe incision, elevation, and removal of the periosteum were done to eliminate spontaneous regeneration potentiality of the defects [21]. Two non-critical sized bone defects [5 mm diameter] were bilaterally produced in the femur bone using dental trephine and a dental drill (Knochenfrasen-Trephine Bur, Germany) [11], as illustrated in [Fig.2]. Left side defects were grafted with MTA and right side defects were grafted with NPCC. At last, the skin flap was relocated and sutured with 4-0 black silk [Ethicon US]. After the procedure, each rabbit was put back in its designated cage after recovering from anesthesia on a heating blanket to

prevent hypothermia. Following surgery, rabbits received 4 mg/kg of carprofen and 5 mg/kg of ceftriaxone for 7 days. Seven days later, the sutures were taken out. Before euthanasia, all surgical sites were visually inspected to evaluate wound healing. Injectable ketamine and xylazine were administered as a premedication. Then, animals were slaughtered at 14 and 28 days in order to extract the femur.

2.3.4. Experimental design

The animals were divided into two groups:

Group I: Consisted of five animals (10 samples) had bilateral femur bone defect and were sacrificed 14 days after the first day of the defects treatment. This group was divided into 2 subgroups:

- *Subgroup Ia (MTA gp):* The left-side femur bone defect was treated using mineral trioxide aggregate, (n= 5 samples).
- *Subgroup Ib (NPCC gp):* The right-side femur bone defect was treated using nano-aragonite powder, (n= 5 samples).

Group II: Consisted of five animals (10 samples) had bilateral femur bone defect and were sacrificed 28 days after the first day of the defects treatment. This group was divided into 2 subgroups:

- *Subgroup IIa (MTA gp):* The left-side femur bone defect was treated using mineral trioxide aggregate, (n= 5 samples).
- *Subgroup IIb (NPCC gp):* The right-side femur bone defect was treated using nano-aragonite powder, (n= 5 samples).

2.3.5. Histopathological assessment

Each femur was dissected and bony blocks enclosing the area of the osseous defect were obtained. All bone blocks were immediately fixed for 72 hours in a buffered 4% formaldehyde solution. Decalcification of the samples was done for about 5 weeks at 4°C using 10% solution of ethylene diamine tetra-acetic acid. The samples were then dehydrated in increasing alcohol grades and cleared from alcohol using xylene. Infiltration and embedding in paraffin wax performed. 5µm thick anteroposterior sections (perpendicular to the defect long axis) were prepared and mounted on glass slides [19]. The sections were stained with hematoxyline and eosin (H&E) and studied by a research light microscope (Olympus® BX 60, Tokyo, Japan)**.**

2.3.6. Radiographic examination

In the present study, radiographic evaluation for both right and left femur of the rabbits was performed after surgical procedures; immediately [base line radiograph], at 14 days and 28 days after the first day of the defect treatment. With the SCANORA 3DX scanner [Scanora 3DX, Soredex, Finland], all CBCT images were obtained. For all photographs taken in the standard resolution mode, the field of view was fixed at 80x 165 mm. 90 kVp and 10 mA were the working settings, and the scanning took roughly 2.4 seconds. A flat panel detector was made of amorphous silicon with an isotropic voxel size of 0.350 mm. Images were analyzed and measurements were taken. To determine relative bone density at the site of the surgical defect, the collected data were exported to the on demand 3D application program (On Demand Cybermed, Co., Seoul, Korea) after being converted to DICOM format. The CBCT scans were evaluated under the guidance of the oral radiologist. In order to test inter-examiner reliability, the examiners were adjusted for the interpretation of the scans and the evaluation was repeated twice within a week.

The examiners discussed any disagreements regarding the measurements until an understanding was obtained [inter-examiner reliability]. The photos could be altered by the examiners to aid in interpretation. Tools for filtration, contrast, magnification, and brightness were employed to improve the measurement processes. The average reading was noted and used for statistical analysis and comparisons between subsequent radiographs [22]. By using the Dental Volume Reformat [DVR] module, relative radiographic bone density was assessed using grayscale value at bone thickness 0.3 mm. The Region Of Interest [ROIs] tool was selected at the surgical defect site was analyzed and the mean values of radio-density was evaluated from axial, cross sectional as well as reformatted panorama of the same module. Bone density was assessed on a scale of 1 to 5 as shown in Table.1 [23].

2.3.7. Statistical analysis

The data was coded and entered using statistical analysis will be performed using the computer program SPSS software for windows version 28.0 (Statistical Package for Social Science, Armonk, NY: IBM Corp). Data were summarized using the mean and standard deviation. For quantitative variables with normally distributed distributions, unpaired t tests were utilized to compare groups and paired sample t test was used to compare time intervals; for non-normally distributed distributions, non-parametric Mann-Whitney tests were performed [10]. A P-value of 0.05 or less was considered statistically significant [23].

3. Result and discussion

3.1. Histopathological Results

****Group I (After 14 days)***

- ***Subgroup Ia (MTA gp)***

After 14 days, H &E sections of MTA group presented areas of fibrovascular tissue with randomly oriented fibroblast-like cells, intense inflammatory infiltrates and numerous dilated congested capillaries in the intrabony defect. Areas of parallel regularly oriented collagen fibers and fibroblast-like cells were also detected. Evidence of endochondral ossification in less vascularized areas was revealed by the presence of a small hyaline cartilaginous zone containing chondroblasts and chondrocytes. Likewise, islands of highly cellular woven bone were detected in higher vascularized areas [Figs. 3a, 3b].

- ***Subgroup Ib (NPCC gp)***

Compared to MTA specimens, the defect area exhibited apparent decrease in the inflammatory reaction and the dilated congested capillaries. Wide fibrovascular tissue with regularly oriented collagen fibers and fibroblast-like cells was observed. Apparently, a larger hyaline cartilaginous area was seen as well as apparently increased woven bone islands lined by osteoblasts and displayed large interposed osteocytes in the intraosseous defect [Figs. 3c, 3d].

****Group II (After 28 days)***

- ***Subgroup IIa (MTA gp)***

MTA group in this experimental period demonstrated partial filling of the defect but with improved osteoblastic and angiogenic activities. An apparent increase

in primitive bone trabeculae that included areas of woven bone as well as mature lamellar bone was observed. The mature bone areas showed apparent decrease of osteoblasts, entrapped osteocytes. Areas of osteoclastic activity were also perceived. Wide marrow cavities with increased vascularity were seen among the bony islands in the defect [Fig. 4a].

- ***Subgroup IIb (NPCC gp)***

In contrast to the MTA group, the specimens of this group revealed enhanced healing features represented by osteogenic and angiogenic activity in bony defect. Defect was entirely filled with fibrovascular, cartilaginous and bony tissues with minimal signs of inflammation. Fibrovascular tissue with regularly oriented collagen fibers and fibroblast-like cells was exhibited besides a considerable area of hyaline cartilage. Primitive trabecular bone extended towards the center of the defect and showed apparently larger areas of highly cellular woven bone together with mature lamellar bone areas, wide marrow cavities and high vascularity. In addition to areas of osteoclastic activity, mature bone areas revealed an apparent decrease in osteoblasts and entrapped osteocytes. A clear boundary between newly primitive trabecular bone and compact bone zone elucidated [Fig. 4b].

3.2. Radiographic Results

Group I (After 14 days)

MTA subgroup showed no calcified tissues with bone density score of [D5] in the bone defect. NPCC subgroup demonstrated a relative increase in bone density within the bone defect giving a bone density score of [D3] (Figs. 5a &5b and Tables 1&2).

Group II (After 28 days)

The MTA subgroup revealed incomplete calcification of the defect size with bone density score of [D3] while NPCC subgroup displayed partial filling of the defect with a thick layer of compact bone showing bone density score [D2] (Figs 5c & 5d and Tables 1&3).

3.3. Statistical Results

Both NPCC and MTA treated femur bone defects showed a significant increase (P value <0.001) in the bone density after 28 days when compared to treated bone defects immediately and after 14 days of treatment respectively. Moreover, NPCC treated defects revealed a high significant increase (P value <0.001) in bone density when compared to MTA treated defects in all periods; immediately, after 14 days and 28 days of treatment (Figs.6,7 & 8 and Tables 2&3).

3.4. Discussion

Bone healing is a complex, multi-step dynamic process that involves coordination of numerous cell types as well as signaling pathways and ensues in different phases. However, auto grafts have dominated in recent decades, and limited clinical application has been reported due to donor bone volume and the difficulties in harvesting activities. Subsequently, several alternatives such bone substitutes are crucial for efficient bone healing. [24]. Rabbits were chosen in the current investigation because they provide more rapid and consistent results than other animals. Faster bone healing has been documented in rabbits, and their genetic characteristics are similar to humans [25]. CBCT imaging analysis is a rapid and nondestructive method that allows three-dimensional assessment of osteogenesis of intrabony defects through quantitative measurement of bone tissue response [22]. Mineral trioxide aggregate (MTA) is biocompatibile when placed in bone tissue, favors tissue regeneration and exhibits a long term prognosis [11].

Nevertheless, a several studies of MTA on its effect on bone regeneration revealed some unsatisfactory results. It was reported that nanomaterials improve bone cells' activities when compared to the micron-sized counterparts for bone repair. Calcium carbonate ($CaCO_3$) is a bone substitute derived from organic sources, such as cuttlefish. Its nanoparticle structure (NPCC) simulates the mineral composition of bone. It is easily prepared and was non-toxic in the animal studies [26]. $CaCO_3$ was used to generate nanoparticles without any additives forming nano-aragonite particles (NPCC) which were used to treat bone defects in rabbit femurs in this study. Therefore, the present study was conducted to histologically and radio graphically (using CBCT) evaluate the osteogenicity of the nano-organite compared with MTA in repairing rabbit femur defects at an interval of 14 and 28 days. H&E sections of MTA-treated femur defects in this study showed few areas of endochondral ossification and woven bone while radio graphically revealing no calcified tissues with [D5] bone density score.

In agreement with these results, MTA was described as highly porous with up to 70% porosity (pore size 250-1000 μm) thus presented an osteoconductive property. Evidences suggested that MTA is associated with direct osteogenic responses in osseous environments including osteoblast attachment, matrix formation, RunX2 expression, and bone apposition [11]. Nonetheless, histological and radiographic results of some previous studies consistent with our results showed that MTA did not promote bone tissue healing due to its chemical composition causing cytotoxicity and accentuated inflammatory infiltrates in early periods. Furthermore, salicylate resin in MTA has been thought to cause apoptosis and radiopacifier bismuth oxide may in turn diminish cellular growth and induce inflammation yet it has been recently replaced by calcium tungstate enhance its biological potentials [27-28]. In comparison to MTA treated defects, the histological results of NPCC treated defects after 14 days in this work exhibited apparent decrease in the inflammatory reaction together with apparently larger hyaline cartilage and increased woven bone islands.

CBCT results ensured histological findings such that a significant increase in bone density with a [D3] score was perceived in NPCC treated defects after 14 days. Accordingly, Green et al. [29], Li et al. [30] and Qianli et al. [31] stated nacre and pearl are natural non-porous composites of highly ordered calcium carbonate crystals cemented by an organic matrix. Aragonite is a crystallization form among three other crystallization forms of nacre and pearl composites. Aragonite nacre or pearl powders were incorporated into scaffold (e.g. poly-L-lactic acid) and used as 3D bio-functional fillers for bone tissue engineering.

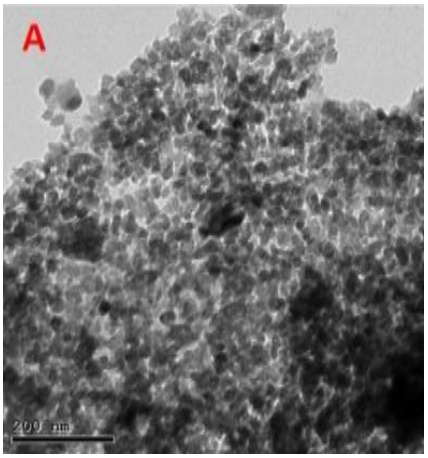

Figure 1. (A) TEM micrographs of nano-aragonite (NPCC) particles; presented regular spherical particles with uniform sizes & average particle size of 25±5nm

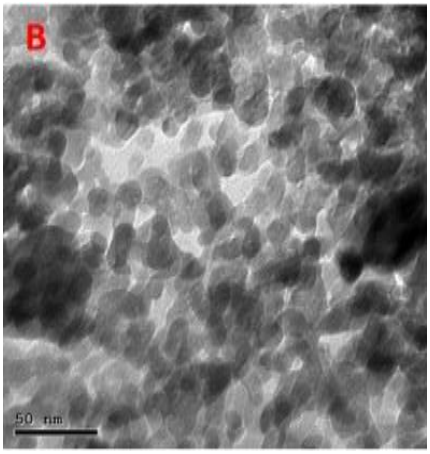

Figure 1. (B) TEM micrographs of nano-aragonite (NPCC) particles; presented regular spherical particles with uniform sizes & average particle size of 25±5nm

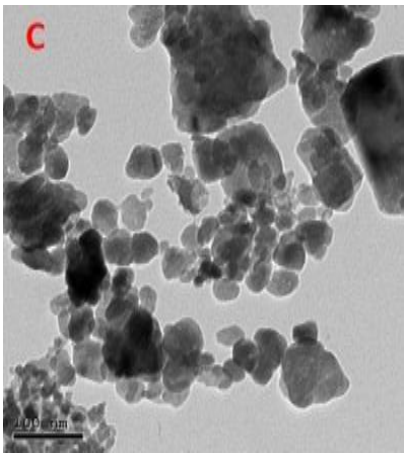

Figure 1. (C) TEM micrographs of nano-aragonite (NPCC) particles; presented regular spherical particles with uniform sizes & average particle size of 25±5nm

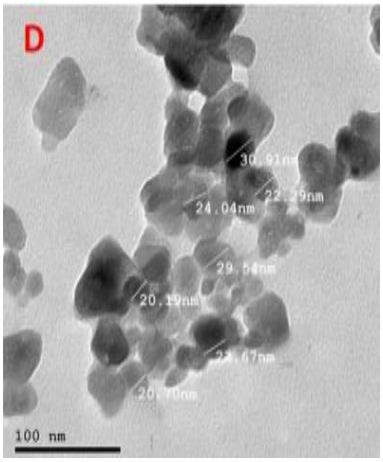

Figure 1. (D) TEM micrographs of nano-aragonite (NPCC) particles; presented regular spherical particles with uniform sizes & average particle size of 25±5nm

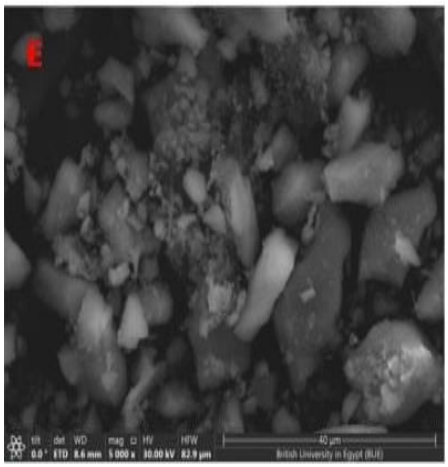

Figure 1. (E) SEM micrographs of nano-aragonite particles displayed diverse forms of “rod shaped” and “spherical” patterns with various surface morphologies

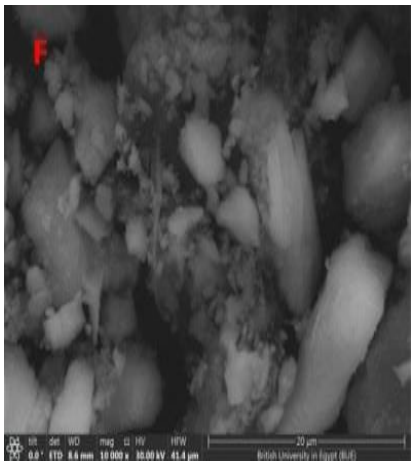

Figure 1. (F) SEM micrographs of nano-aragonite particles displayed diverse forms of “rod shaped” and “spherical” patterns with various surface morphologies

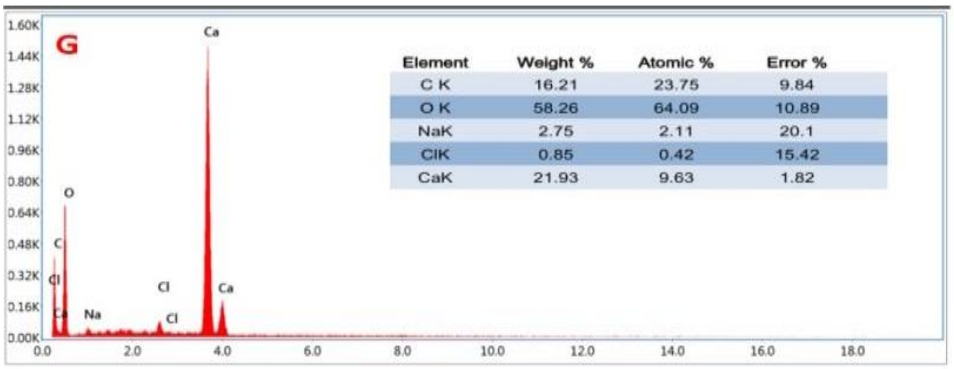

Element	Weight %	Atomic %	Error %
C K	16.21	23.75	9.84
O K	58.26	64.09	10.89
NaK	2.75	2.11	20.1
ClK	0.85	0.42	15.42
CaK	21.93	9.63	1.82

Figure 1. (G) EDX analysis for elemental composition of NPCC

Figure 2. A photograph showing a disinfected surgical bony defect in a rabbit femur.

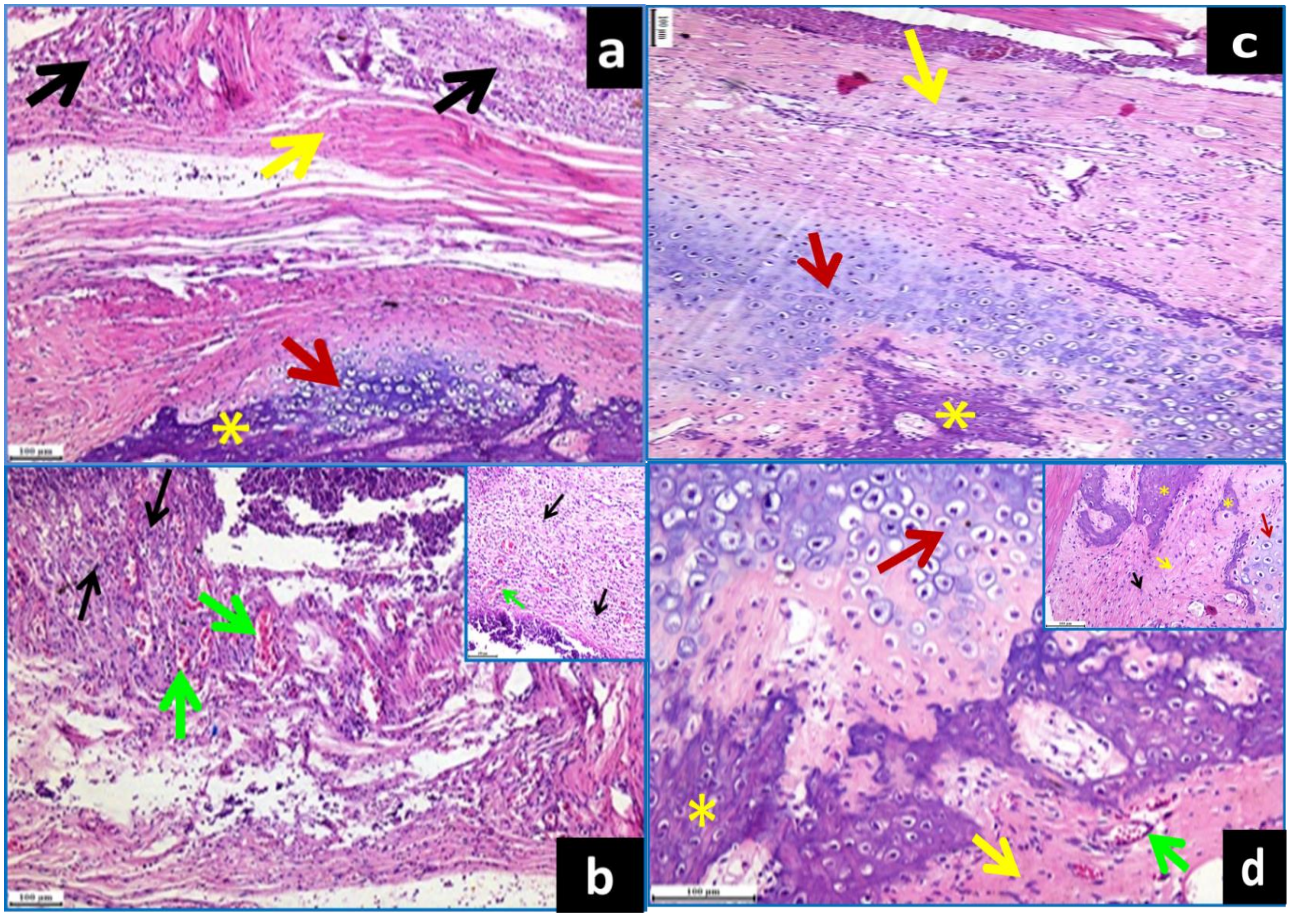

Figure 3. Photomicrographs of treated intrabony defect in a rabbit femur after 14 days (Group I), (a, b) MTA subgroup and (c,d) NPCC subgroup; (a) MTA subgroup showed fibrovascular tissue, areas of regularly oriented collagen fibers, a small hyaline cartilaginous area, islands of highly cellular woven bone (H&E, X100), (b) intense inflammatory infiltrates & dilated congested capillaries(H&E, X200 ; Inset: X400), (c) NPCC subgroup displayed wide fibrovascular tissue, apparent decrease in inflammatory reaction & dilated congested capillaries & apparently larger hyaline cartilage (H&E, X100), (d) apparent increase in woven bone islands lined by osteoblasts and displayed large interposed osteocytes (H&E, X200 ; Inset: X400), fibrovascular tissue (yellow arrows), Inflammatory reaction (black arrows), blood vessels (green arrows), hyaline cartilage (red arrows), woven bone (yellow asterisk).

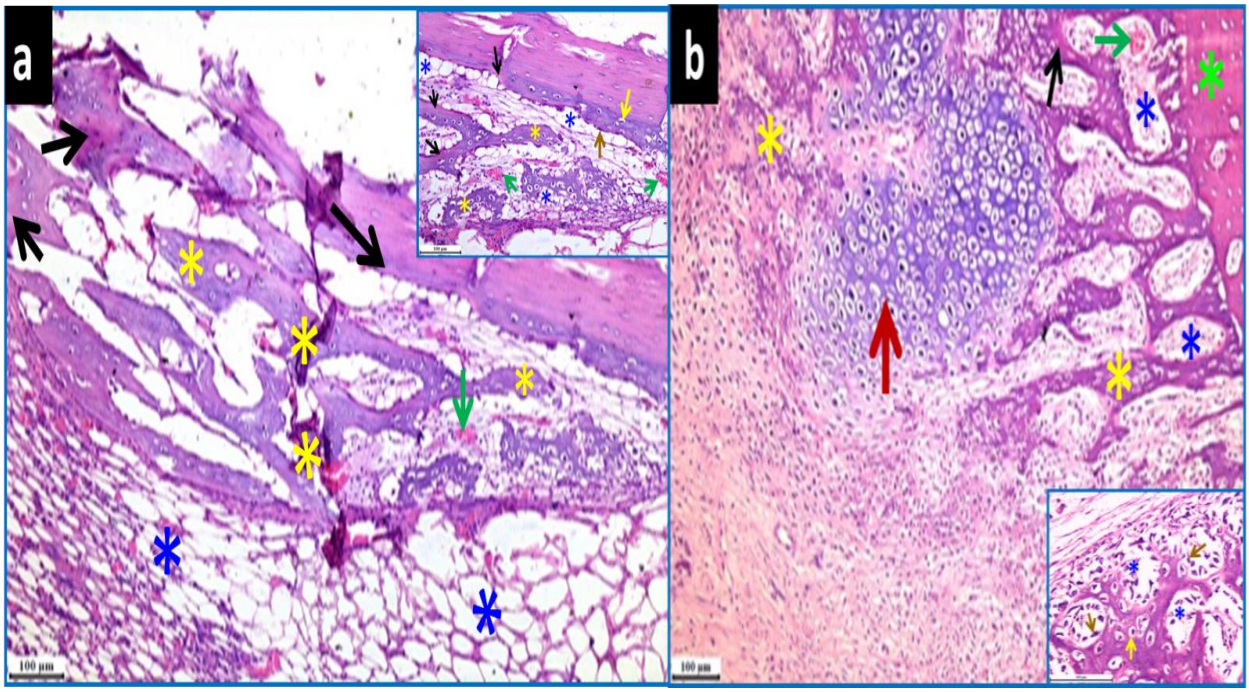

Figure 4. Photomicrographs of treated intrabony defect in a rabbit femur after 28 days (Group II), (a) MTA subgroup exhibited an apparent increase in woven bone & mature lamellar bone areas with an apparent decrease of osteoblasts & osteocytes, wide marrow cavities with increased vascularity (H&E, X200), (b) NPCC subgroup showed wide fibro vascular tissue, a considerable cartilaginous area, apparently larger areas of highly cellular woven bone with osteoblasts, large osteocytes, wide marrow cavities & increased vascularity (Inset; X400) , areas of mature lamellar bone, a boundary between primitive bone & compact bone zone was seen (H&E, X200), woven bone (yellow asterisks), mature lamellar bone (black arrows), marrow cavities (blue asterisks), hyaline cartilage (red arrow), compact bone (green asterisk), blood vessels (green arrows), osteoblasts (brown arrows), osteocytes (yellow arrows).

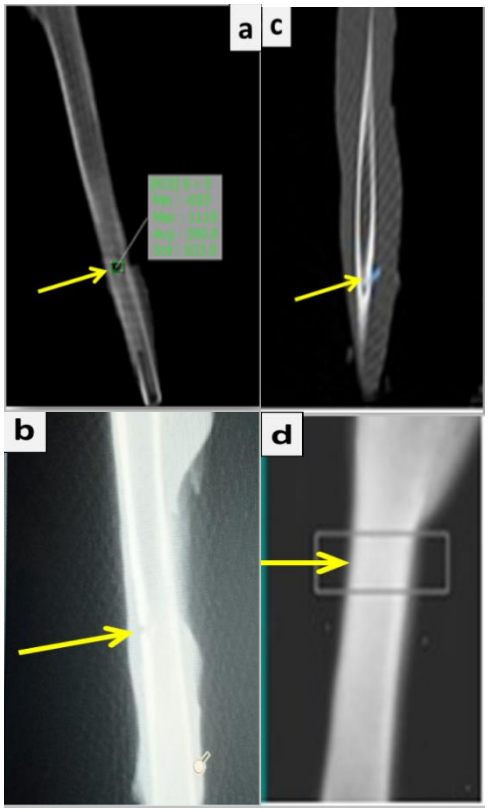

Figure 5. Axial cut of cone beam computed tomography (CBCT) of the femoral defect in a rabbit model at both time periods [14 days and 28 days], (a) MTA group showed the surgical defect after 14 days, (b) MTA group displayed the opacification of the surgical defect after 28 days, (c) NPCC group presented the surgical defect after 14 days, (d) NPCC group exhibited opacification & increased bone density of the surgical defect after 28 days.

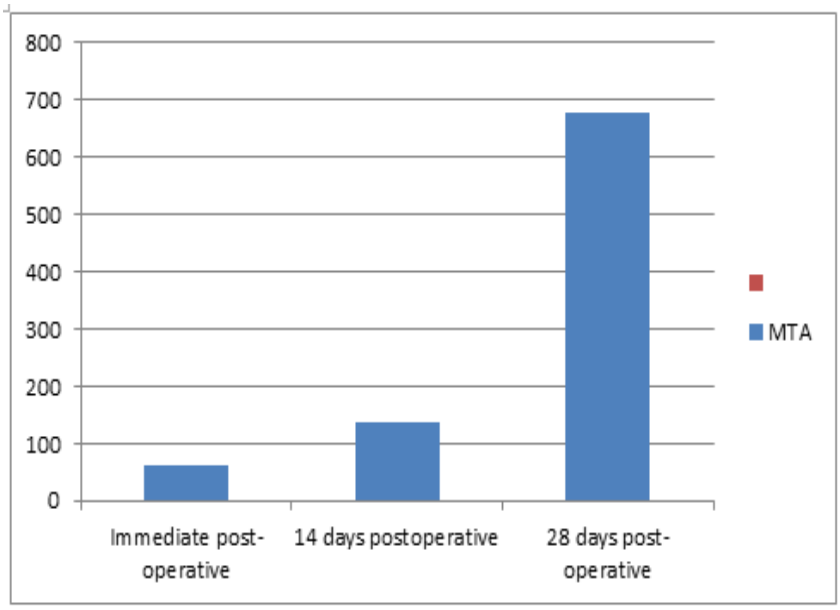

Figure 6. Bar chart showing mean +SD of bone density in MTA group immediately, 14 days & 28 days post-operative.

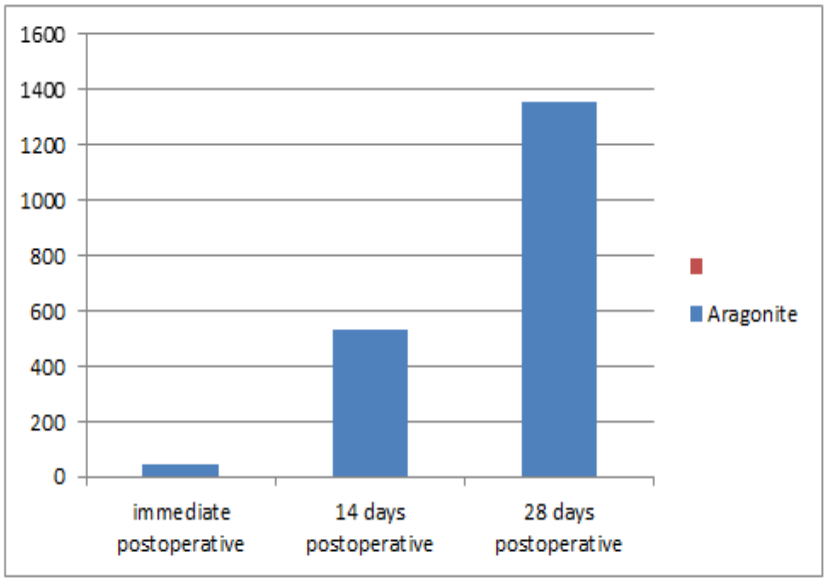

Figure 7. Bar chart showing mean +SD of bone density in NPCC group immediately, 14 days & 28 days post-operative.

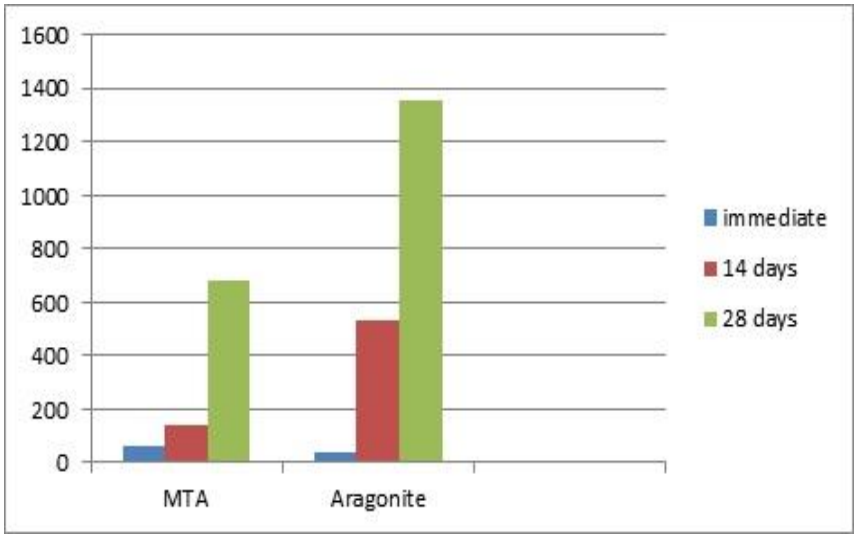

Figure 8. Bar chart showing mean +SD of bone density in MTA & NPCC groups immediately, 14 days & 28 days post-operative.

Table 1. The radiographic score of bone defect

Type of bone	CT value	Comments
D1	> 1250 HU	Homogenous and compact bone.
D2	850-1250 HU	A thick layer of compact bone surrounding a core of dense trabecular bone.
D3	350-850 HU	A thin layer of cortical bone surrounding a dense trabecular bone of favorable strength.
D4	150-350 HU	A thin layer of cortical bone surrounding a core of low density trabecular bone.
D5	< 150 HU	Very soft bone with incomplete mineralization.

Table 2. Bone density of the femoral defect in the MTA and NPCC groups immediately and 14 days post-operative

	MTA		Aragonite		
	Mean	**Standard Deviation**	**Mean**	**Standard Deviation**	**P value**
Immediate post-operative	61	12.91	41.95	9.78	0.029**
14 days post-operative	138.7	15.51	529.83	13.82	<0.001**
P value	<0.001**		<0.001**		

**; mean significant difference at P≤0.05.

Table 3. Bone density of the femoral defect in the MTA and NPCC groups immediately and 28 days post-operative

	MTA		Aragonite		
	Mean	**Standard Deviation**	**Mean**	**Standard Deviation**	**P value**
Immediate post-operative	61	15.44	41.95	4.25	0.786
28 days post-operative	678.4	14.75	1357.73	12.32	<0.001
P value	<0.001**		<0.001**		

**; mean significant difference at P≤0.05.

Moreover, it was proposed that the alkaline microenvironment (pH 7.8–8.5) and Ca^{2+} concentration in aragonite composite filler resulted from the dissolution of $CaCO_3$ is tolerant for induction of osteoblastic activity [32-33]. Therefore, Maeno et al. found that 2-4 mM Ca^{2+} was ideal for osteoblast survival and proliferation whereas 6-8 mM Ca^{2+} was favorable for osteoblast maturation and matrix mineralization [34]. Regarding the histological results of the treated defects after 28 days of ongoing work, the MTA group displayed partial filling of the non-critical sized femur defect. Improved osteogenesis was represented by an apparent increase in woven and mature lamellar bone areas. CBCT data supported these findings exhibiting incomplete calcification of the defect with a significant increase and [D3] bone density score compared to 14 days MTA treated defect. Concurrently, in assessing bone tissue responses to MTA, several studies [11-28-35-36] documented minimal or absent inflammatory responses after 4, 6 and 8 weeks in bone defects treated with MTA. For bone cells, MTA acts as a bioactive substrate and promotes the production of cytokines like interleukin. It is necessary to improve the potency of MTA in bone regeneration by combining it with calcium hydroxide for example. Especially that the amount of induced bone repair and new bone growth was not significant when using MTA.

Compared to MTA-treated defects in the current work after 28 days, H&E stained NPCC treated defects were entirely filled with fibro vascular, cartilaginous and bony tissues with minimal or no signs of inflammation. This indicates the increased osteogenic and angiogenic activities as well as enhanced bone repair denoted by apparently larger areas of woven bone and mature lamellar bone including a compact bone zone. Likewise, CBCT revealed a thickened zone of compact bone with a significant increase and [D2] bone density score when compared to 14 days NPCC treated defects and to 14 and 28 days MTA treated defects.In harmony with these histological and CBCT findings, it was clarified that NPCC powder is comparable to bone and was difficult to be distinguished from the surrounding bone after 30 days as it stimulated bone formation and was replaced by new bone that eventually merged with the pre-existing bone [37-38]. Qianli et al. [31] disclosed significant bone regeneration with typical endochondral ossification after 4 weeks. Moreover, in vitro study of Asvanund et al. showed that $CaCO_3$ crystals increased the formation of bone sialoprotein and alkaline phosphatase by human bone cells after 4 weeks of treatment implying the greatest potential of bone formation and maturation [37].

4. Conclusions

The histological and CBCT investigations proved that nano-aragonite powder was superior to mineral trioxide

aggregate in osteogenesis, mineralization potential and, bone regeneration of non-critical sized defects. This can be attributed to the existence of osteogenic molecules within the organic matrix. Further modifications of nanoaragonite powder are recommended to enhance its osteoinductivity in addition to its osteoconductivity. At that time, nano-aragonite powder can be used a a natural and functional bone substitute in non-critical and critical-sized bone defects. Additionally, more clinical trials are mandatory to assess the sustainability of nano-aragonite powder.

Funding

Open access funding provided by The Science, Technology & Innovation Funding Authority (STDF) in cooperation with The Egyptian Knowledge Bank (EKB).

Competing interests

The authors declare no competing interests.

Consent for publication

Not applicable according to the ethical committee at Faculty of Dentistry, Suez Canal University, Egypt.

Data availability

The datasets generated and analyzed during the current study are available from the corresponding author on reasonable results.

References

[1] K.A. Al Ruhaimi. (2000). Effect of adding resorbable calcium sulfate to grafting materials on early bone regeneration in osseous defects in rabbits. International Journal of Oral & Maxillofacial Implants. 15(6).

[2] E.S. Apaydin, M. Torabinejad. (2004). The effect of calcium sulfate on hard-tissue healing after periradicular surgery. Journal of endodontics. 30(1): 17-20.

[3] E. Carneiro, R.B. Garcia. (2003). Análise microscópica descritiva do efeito do tamanho das partículas de matriz de osso medular bovino desmineralizado na reparação de defeito ósseo em fêmures de coelhos.

[4] J.C. Zielak, I. Vendramini, P.F.C.d.L. Corso, L.L. Muller, V.R. Crivellaro, S.S. Khajotia, F.L. Esteban Florez, R. Scariot, M. Elsalanty, T.M. Deliberador. (2020). The Role of Marine Organic Extract in Bone Regeneration: A Pilot Study. BioMed Research International. 2020(1): 2925879.

[5] L. Addadi, S. Raz, S. Weiner. (2003). Taking advantage of disorder: amorphous calcium carbonate and its roles in biomineralization. Advanced materials. 15(12): 959-970.

[6] Z.P. Xu, Q.H. Zeng, G.Q. Lu, A.B. Yu. (2006). Inorganic nanoparticles as carriers for efficient cellular delivery. Chemical Engineering Science. 61(3): 1027-1040.

[7] H. Peng, Y. Han, T. Liu, W.C. Tjiu, C. He. (2010). Morphology and thermal degradation behavior of highly exfoliated CoAl-layered double hydroxide/polycaprolactone nanocomposites prepared by simple solution intercalation. Thermochimica Acta. 502(1-2): 1-7.

[8] J. Rocha, A. Lemos, S. Agathopoulos, P. Valério, S. Kannan, F. Oktar, J. Ferreira. (2005). Scaffolds for bone restoration from cuttlefish. Bone. 37(6): 850-857.

[9] D. Milovac, T.C. Gamboa-Martínez, M. Ivankovic, G.G. Ferrer, H. Ivankovic. (2014). PCL-coated hydroxyapatite scaffold derived from cuttlefish bone: In vitro cell culture studies. Materials Science and Engineering: C. 42: 264-272.

[10] Y. Chan. (2003). Biostatistics 102: quantitative data–parametric & non-parametric tests. blood Press. 140(24.08): 79.

[11] G.M. Galal, S.S. Abd El Rehim, S.S. Karam. (2019). The effect of mineral trioxide aggregate alone and in combination with biphasic calcium phosphate on healing of mandibular defects in rabbit. Alexandria Dental Journal. 44(3): 77-81.

[12] T. Komabayashi, Q. Zhu. (2010). Innovative endodontic therapy for anti-inflammatory direct pulp capping of permanent teeth with a mature apex. Oral Surgery, Oral Medicine, Oral Pathology, Oral Radiology, and Endodontology. 109(5): e75-e81.

[13] A.L. Pinheiro, L.G. Soares, A.F. Barbosa, L.M. Ramalho, J.N. dos Santos. (2012). Does LED phototherapy influence the repair of bone defects grafted with MTA, bone morphogenetic proteins, and guided bone regeneration? A description of the repair process on rodents. Lasers in Medical Science. 27: 1013-1024.

[14] J. Camiletti, A.M. Soliman, M.L. Nehdi. (2013). Effect of nano-calcium carbonate on early-age properties of ultra-high-performance concrete. Magazine of Concrete Research. 65(5): 297-307.

[15] Y. Josset, Z. Oum'Hamed, A. Zarrinpour, M. Lorenzato, J.-J. Adnet, D. Laurent–Maquin. (1999). In vitro reactions of human osteoblasts in culture with zirconia and alumina ceramics. Journal of Biomedical Materials Research: An Official Journal of The Society for Biomaterials, The Japanese Society for Biomaterials, and The Australian Society for Biomaterials and the Korean Society for Biomaterials. 47(4): 481-493.

[16] E. Roberts, L. Poon, R. Smith. (1986). Interface histology of rigid endosseous implants. The Journal of Oral Implantology. 12(3): 406-416.

[17] J.-G. Barth. (2020). Limestone and calcium in plants. Elemente der Naturwissenschaft. 112: 29-78.

[18] T. Fernandez-Medina, A. Nanda. (2021). Regeneration for implant dentistry. Regenerative Approaches in Dentistry: An Evidence-Based Perspective. 133-150.

[19] A.Z. Abdelaal, F. Saad. (2021). Estimation of the therapeutic effect of diode laser on bone cells in mandibular distraction osteogenesis: An experimental study in adult male rabbits. Egyptian Journal of Histology. 44(4): 902-915.

[20] F. Faul, E. Erdfelder, A.-G. Lang, A. Buchner. (2007). G* Power 3: A flexible statistical power analysis program for the social, behavioral, and

biomedical sciences. Behavior research methods. 39(2): 175-191.

[21] M. Wang, X. Zhang, Y. Li, A. Mo. (2021). The influence of different guided bone regeneration procedures on the contour of bone graft after wound closure: a retrospective cohort study. Materials. 14(3): 583.

[22] A. Ewald, A. Fuchs, L. Boegelein, J.-P. Grunz, K. Kneist, U. Gbureck, S. Hoelscher-Doht. (2023). Degradation and bone-contact biocompatibility of two drillable magnesium phosphate bone cements in an in vivo rabbit bone defect model. Materials. 16(13): 4650.

[23] A. Khaohoen, T. Sornsuwan, P. Chaijareenont, P. Poovarodom, C. Rungsiyakull, P. Rungsiyakull. (2023). Biomaterials and clinical application of dental implants in relation to bone density—A narrative review. Journal of clinical medicine. 12(21): 6924.

[24] T.M.A. Alfar Sr, W.S. Alaida, H.A. Hammudah, L.L. Mohamado, R.R. Gaw, L. Al-Salamah, B.A. Alasmari, R.M. Alotaibi, M.A. Almutairi. (2023). Exploring the Potential of Phytogenic Materials for Bone Regeneration: A Narrative Review of Current Advances and Future Directions. Cureus. 15(11).

[25] M. Miloro, D.J. Haralson, V. Desa. (2010). Bone healing in a rabbit mandibular defect using platelet-rich plasma. Journal of Oral and Maxillofacial Surgery. 68(6): 1225-1230.

[26] S.M. Gadallah, M. Abd-Elkawi, T.N. Misk, A.M. Sharshar. (2022). The efficacy of nano-calcium carbonate derived from coral reefs and nano-silver to induce new bone formation in critical radial bone defect in rabbits: Radiological evaluation. Journal of Current Veterinary Research. 4(2): 113-123.

[27] S. Jung, S. Sielker, M.R. Hanisch, V. Libricht, E. Schäfer, T. Dammaschke. (2018). Cytotoxic effects and differentiation in monolayer and 3D culture. Biomaterials. 26(23): 4847-4855.

[35] M.G. Torreira, A. Dos Santos, M.R. Cobos, I.F. Boquete, A.C. Abelleira. (2004). The osteoinductive potential of MTA (Mineral trioxide aggregate): a histologic study in rabbits. Eur J Anat. 8(3): 101-5.

[36] R.P. McNamara, M.A. Henry, W.G. Schindler, K.M. Hargreaves. (2010). Biocompatibility of of four different root canal sealers on human osteoblasts. PLoS One. 13(3): e0194467.

[28] M.M. Delfino, J.M. Guerreiro-Tanomaru, M. Tanomaru-Filho, E. Sasso-Cerri, P.S. Cerri. (2020). Immunoinflammatory response and bioactive potential of GuttaFlow bioseal and MTA Fillapex in the rat subcutaneous tissue. Scientific reports. 10(1): 7173.

[29] D.W. Green, H.-J. Kwon, H.-S. Jung. (2015). Osteogenic potency of nacre on human mesenchymal stem cells. Molecules and cells. 38(3): 267-272.

[30] X. Li, X. Yang, X. Liu, W. He, Q. Huang, S. Li, Q. Feng. (2018). Calcium carbonate nanoparticles promote osteogenesis compared to adipogenesis in human bone-marrow mesenchymal stem cells. Progress in Natural Science: Materials International. 28(5): 598-608.

[31] Q. Huang, Y. Liu, Z. Ouyang, Q. Feng. (2020). Comparing the regeneration potential between PLLA/Aragonite and PLLA/Vaterite pearl composite scaffolds in rabbit radius segmental bone defects. Bioactive materials. 5(4): 980-989.

[32] J. Tan, D. Wang, H. Cao, Y. Qiao, H. Zhu, X. Liu. (2018). Effect of local alkaline microenvironment on the behaviors of bacteria and osteogenic cells. ACS applied materials & interfaces. 10(49): 42018-42029.

[33] Q. Li, D. Wang, J. Qiu, F. Peng, X. Liu. (2018). Regulating the local pH level of titanium via Mg–Fe layered double hydroxides films for enhanced osteogenesis. Biomaterials science. 6(5): 1227-1237.

[34] S. Maeno, Y. Niki, H. Matsumoto, H. Morioka, T. Yatabe, A. Funayama, Y. Toyama, T. Taguchi, J. Tanaka. (2005). The effect of calcium ion concentration on osteoblast viability, proliferation accelerated mineral trioxide aggregate in a rat model. Journal of endodontics. 36(11): 1851-1855.

[37] P. Asvanund, P. Chunhabundit. (2012). Alveolar bone regeneration by implantation of nacre and B-tricalcium phosphate in guinea pig. Implant dentistry. 21(3): 248-253.

[38] L. Leelatian, P. Chunhabundit, P. Charoonrut, P. Asvanund. (2022). Induction of osseointegration by nacre in pigs. Molecules. 27(9): 2653.